

A theoretical analysis of flux-qubit measurements with a dc-SQUID

Hayato Nakano^{1,3}, Hirofumi Tanaka^{1,3}, Shiro Saito^{1,3}, Kouichi Semba^{1,3}, Hideaki Takayanagi^{1,3}, and Masahito Ueda^{2,3}

¹NTT Basic Research Laboratories, NTT Corporation, Atsugi-shi, Kanagawa 243-0198, Japan.

²Tokyo Institute of Technology, Meguro-ku, Tokyo 152-8551, Japan.

³CREST, Japanese Science and Technology Agency

The readout process of a superconducting flux-qubit is theoretically analyzed in terms of the quantum dynamics of a qubit-SQUID coupled system during measurement. The quantity directly observed by the measurement is the switching current (I_{sw}) of the dc-SQUID placed around the qubit ring. In order to clarify the relation between the I_{sw} and the qubit state, we calculated the time evolution of the density operator of the qubit-SQUID system while increasing the SQUID bias current until switching events occur and obtained the switching current distributions. This clarifies what information of the qubit is obtained by a dc-SQUID switching current measurement under specific conditions, for example, when the qubit eigenstate is a superposition of two different flux states.

PACS numbers: 85.25.Dg, 03.67.Mn, 03.65.Yz

I. INTRODUCTION

The quantum bit (qubit) is the fundamental element of quantum computers¹. Recently, many experiments have been reported on quantum two-state systems consisting of superconducting circuits with Josephson junctions^{2,3,4,5,6,7,8,9,10}. Some of these systems use two flux-states in the superconducting ring that are macroscopically distinguishable from each other, and the superposition of these two states^{2,3,5,6,10}. These are called superconducting flux-qubits. The two states can be characterized by the directions of the circulating supercurrent along the ring, and the magnetic flux that is induced by the supercurrent.

In experiments, small magnetic-field measurements made with dc-SQUIDs are used to read out the flux qubit states. A dc-SQUID is a highly sensitive magnetic flux probe. The measurement result is the bias current at which the SQUID switches to the voltage state. The switching current (I_{sw}) of the SQUID varies depending on the quantum state of the qubit.

The qubit ring has two stable states. One induces the flux $+\Phi_0$, and the other $-\Phi_0$. The SQUID switches at a bias current of $I_{sw} = I_{c0} \cos[(\Phi_{SQ} - \Phi_0)/\Phi_0]$ depending on which state the ring is in. Here, Φ_{SQ} is the external flux applied to the SQUID ring, and $\Phi_0 = h/(2e)$ is the flux quantum. Therefore, at $\Phi_{SQ} = 0 = 1/2\Phi_0$, where the two states are energetically degenerated, the switching current appears probabilistically at I_{sw+} or I_{sw-} for each measurement in the sense of classical statistics.

When Josephson junctions in the ring are small enough the ring becomes a quantum two-state system, that is, a qubit. Then, it is not so trivial what is meant by the obtained switching current, especially when the qubit is not in an eigenstate of the quantity measured by the SQUID.

There are at least two possibilities. A first possibility is that the dc-SQUID measurements of flux-qubits is a projection measurement of the small flux induced by the qubit ring current. The qubit has only two states

where the current is definite. The switching current appears probabilistically at I_{sw+} or I_{sw-} even when the qubit state is a superposition of the two possible states before the measurement. Then, after the measurement, the qubit state jumps to the one of the two states corresponding to the measurement result. A second possibility is that the switching current has an intermediate value between I_{sw+} and I_{sw-} and does not behave probabilistically even for a qubit that is in a superposition state.

In experiments, when the fluctuation of the switching current is larger than $|I_{sw+} - I_{sw-}|$ and when we need to take the average of many measured switching current values in order to determine the qubit-inducing flux, it is impossible to distinguish which of the two possibilities above is correct because the averaged values always appear between I_{sw+} and I_{sw-} independent of the possibilities and never behave probabilistically. To clarify what each switching current obtained by each measurement corresponds to, and what is meant by the distribution of a huge number of measured switching currents, we must undertake a quantitative analysis of the dynamics of the whole system, which consists of the measured object (flux qubit) and the measurement apparatus (dc-SQUID).

The rest of this paper is organized as follows. Section II briefly introduces the background to superconducting flux-qubit measurement with a dc-SQUID. Section III shows the Hamiltonian of the flux-qubit and dc-SQUID coupled system, and derives a simplified version, which is applicable to numerical calculations. Section IV describes our numerical calculation of the time evolution of the density operator of the qubit-SQUID composite system. Section V shows the results of the calculations and discusses them. Section VI makes some concluding remarks.

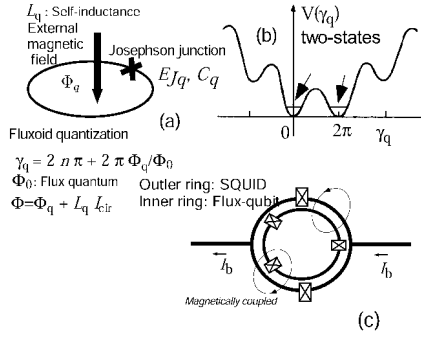


FIG. 1: Principle of the flux qubit. (a) Superconducting ring and flux quantization. (b) Potential energy for the Josephson phase γ_q and the two states. (c) Geometry of the dc-SQUID and the flux qubit for the measurement setup.

II. FLUX-QUBIT AND READING OUT OF STATES WITH A DC-SQUID.

A. Superconducting flux-qubits

A superconducting flux qubit is a superconducting ring interrupted by a Josephson junction (or junctions). The flux quantization causes the junction phase difference γ_q and the external flux Φ_q applied by the magnetic field to obey the condition such that

$$\gamma_q = 2\pi n + 2\pi \frac{\Phi_q}{\Phi_0}; \quad (1)$$

where $\Phi_q = \Phi_q + L_q I_{cir}$, n is an integer, and I_{cir} is the circulating supercurrent along the ring [Fig. 1(a)].

Suppose that an external flux $\Phi_q = (n+1/2)\Phi_0$ pierces the qubit ring. The two states in the wells, $\gamma_q = n\pi$ and $\gamma_q = (n+1)\pi$, of the potential energy $V(\gamma_q)$ are energetically degenerate [Fig. 1(b)]. We denote these two states by $|L\rangle$ and $|R\rangle$. The Josephson plasma oscillation energy $\hbar J_p = 2E_C E_J$ gives approximate level splitting in each well, where $E_C = (2e)^2/(2C_q)$ and E_J are the charging energy and the Josephson energy of the junction, respectively. When the potential barrier at $\gamma_q = (n+1/2)\pi$ is comparable to the charging energy E_C , macroscopic quantum tunneling of the phase couples states between the barrier. When the anti-crossing energy separation between the coupled states are much smaller than the level splitting $\hbar J_p$, two states, those are energetically nearest and in different wells, are almost independent other states. Then, we can consider these two states as a two-state system, that is, a qubit.

We can treat the states of the ring as a pseudo two-level system and obtain a reduced two-level-system Hamiltonian with a $|L\rangle, |R\rangle$ basis:

$$H_q = \frac{1}{2} \begin{pmatrix} \epsilon_L & \epsilon_R \end{pmatrix} \begin{pmatrix} |L\rangle & |R\rangle \end{pmatrix} \quad (2)$$

where 2ϵ is the energy difference between the localized states in the left and right wells and can be controlled by

an external magnetic field. Here, ϵ represents the transfer energy due to macroscopic quantum tunneling between the wells, and

$$\begin{aligned} z &= \begin{pmatrix} \epsilon_L & \epsilon_R \\ 0 & 0 \end{pmatrix} \\ x &= \begin{pmatrix} \epsilon_L & \epsilon_R \\ \epsilon_R & \epsilon_L \end{pmatrix} \end{aligned} \quad (3)$$

The eigenenergy of the ground (excited) states of Hamiltonian 2 is given by $E_{g(e)} = \frac{1}{2}(\epsilon_L + \epsilon_R \pm \sqrt{\epsilon_L^2 + \epsilon_R^2})$. The eigenstates are

$$\begin{aligned} |g\rangle &= \frac{1}{\sqrt{2}} \begin{pmatrix} |L\rangle + |R\rangle \end{pmatrix} \\ |e\rangle &= \frac{1}{\sqrt{2}} \begin{pmatrix} |L\rangle - |R\rangle \end{pmatrix} \end{aligned} \quad (4)$$

where $\tan[\theta] = \epsilon_R/\epsilon_L$. The energy levels exhibit anti-crossing at $\Phi_q = (n+1/2)\Phi_0$ due to the mixing of $|L\rangle$ and $|R\rangle$ via macroscopic quantum tunneling. The quantum mechanical average of the qubit circulating current $\langle I_{cir} \rangle = I_{c0} \langle \sin \gamma_q \rangle$ ($i = g, e$), for the ground $|g\rangle$ and the first excited states $|e\rangle$, can be obtained using $\langle \sin \gamma_q \rangle = \frac{1}{\sqrt{2}} \cos \theta$ and $\langle \sin \gamma_q \rangle = \frac{1}{\sqrt{2}} \sin \theta$, where I_{c0} is the maximum supercurrent along the qubit ring.

B. Measurement with dc-SQUID

The "readout" of the flux qubit is the result of measurement to determine whether the qubit is in the $|L\rangle$ or $|R\rangle$ state. The difference between them, which is measurable from the outside, is the direction of the circulating supercurrent along the ring and the magnetic field induced by the current. The field changes its sign depending on the states $|L\rangle$ and $|R\rangle$. Then, we expect that, by measuring the field with a dc-SQUID, we can distinguish the state of the qubit. This method is actually used in the experiments.

The switching current I_{sw} of the SQUID is the bias current value at which the sum of the macroscopic phase differences of two junctions, $\phi_1 + \phi_2 = 2\pi$, escapes from the potential well. In a classical situation, where the external flux Φ_{SQ} is added and a small flux Φ_q is induced in the SQUID ring, the switching current is $I_{sw}(\Phi_q) = I_0 \cos[\phi_{SQ} = 0] - \frac{I_0}{2} \sin[\phi_{SQ} = 0]$, where $I_0 = \frac{2e}{\hbar} E_{J0}$, and E_{J0} is the Josephson coupling energy of the junction. In real qubit measurements, the induced flux is $10^{-3} \Phi_0$ to $10^{-2} \Phi_0$.

This type of quantum superposition state is called as macroscopic quantum coherence (MQC). The question of whether MQC is actually possible, was originally introduced by A. J. Leggett, in the 1980's¹³. Recently MQC has been experimentally observed in a superconducting ring with Josephson junctions⁶. This MQC can also be used as a qubit because it is a typical two-state quantum system with controllable parameters. A qubit based on

since the energy-level spacing of these harmonic oscillators is very wide, the contributions, which are non-local in time, are negligible and we obtain a simplified Hamiltonian for the total system as

$$H^0 = H_q^0 + H_{SQ}^0 + H_{int}^0 \quad (11)$$

where

$$H_q^0 = \frac{\hbar^2}{2e} \frac{C_q}{4} \frac{\partial^2}{\partial q^2} + \frac{\partial^2}{\partial q} + 2 \frac{\partial^2}{\partial q} \quad (12)$$

$$2E_J \cos[q_+ = 2] \cos[q_- = 2] - E_J \cos[q_- = 2 f_q];$$

$$H_{SQ}^0 = \frac{\hbar^2}{2e} \frac{C_0}{4} \frac{\partial^2}{\partial q^2} - 2E_{J0} \cos[q_+ = 2] \cos[q_{SQ}] \quad (13)$$

$$\frac{\hbar}{2e} I_b(t) \frac{\partial}{\partial q};$$

$$H_{int}^0 = \frac{1}{2L_q} \frac{2e}{\hbar} \frac{\partial^2}{\partial q^2} \quad (14)$$

$$[(L_q E_J \sin[q_- = 2 f_q] + M E_{J0} \cos[q_+ = 2] \sin[q_{SQ}])^2 - (L_q L - M^2) (E_{J0} \cos[q_+ = 2] \sin[q_{SQ}])^2]$$

Here we disregarded E_{J0} , E_J compared with $(\hbar = (2e))^2 = L_q$, $(\hbar = (2e))^2 = L$ because the inductances (L and L_q) are small in experimental situations.

2. Two-state approximation of the qubit

To achieve further simplification we have to calculate the quantum states of the three junction qubit using the Hamiltonian Eq. (12) with realistic parameters. In the vicinity of $f_q = 1/2$, Eq. (12) becomes

$$H_q^0 = H_0 + H_1; \quad (15)$$

where

$$H_0 = \frac{\hbar^2}{2e} \frac{C_q}{4} \frac{\partial^2}{\partial q^2} + \frac{\partial^2}{\partial q} + 2 \frac{\partial^2}{\partial q} \quad (16)$$

$$2E_J \cos[q_+ = 2] \cos[q_- = 2] + E_J \cos[q_-];$$

and

$$H_1 = E_J \sin[q_-] 2 f; \quad (17)$$

with $f = f_q - 1/2$. Here, we ignored f^2 and higher powers because f_q is always in the vicinity of $1/2$ ($0.499 < f_q < 0.501$) in ux-qubit experiments. Since H_0 has an even symmetry about q_- and has potential wells on the both sides of $q_- = 0$, when $H_1 = 0$, that is, when $f = 0$,

the ground state $|j_i\rangle$ and the first excited state $|j_i\rangle$ can be expressed as

$$|j_i\rangle = (|j_i\rangle + |j_i\rangle) \frac{1}{\sqrt{2}}; \quad (18)$$

$$|j_i\rangle = (|j_i\rangle - |j_i\rangle) \frac{1}{\sqrt{2}};$$

where $|j_i\rangle$ and $|j_i\rangle$ are wavefunctions approximately localized in the left and right wells, respectively. When other excited states are adequately higher than these states in terms of energy, this is a two-state system.

For finite but very small f , we can carry out a second-order perturbation calculation by adopting H_1 as a perturbation because $f = f_q - 1/2$ is very small. Then we obtain the perturbed ground and excited states by the first order of perturbations as

$$|j_i\rangle = |j_i\rangle + \frac{2 f E_J}{E_i} \frac{\langle j_i | H_1 | j_i \rangle}{E_i} |j_i\rangle + \frac{P}{E_i} \frac{\langle j_i | H_1 | j_i \rangle}{E_i} |j_i\rangle; \quad (19)$$

$$|j_i\rangle = |j_i\rangle + \frac{2 f E_J}{E_i} \frac{\langle j_i | H_1 | j_i \rangle}{E_i} |j_i\rangle + \frac{P}{E_i} \frac{\langle j_i | H_1 | j_i \rangle}{E_i} |j_i\rangle;$$

where $|j_i\rangle$ and E_i is a second or higher excited state and its energy when there is no perturbation. The qubit is always operated under the condition that the second and higher excited states are energetically far from $|j_i\rangle$ and $|j_i\rangle$, $E_i \gg E_i - 2 f$ are always satisfied. Therefore, the third terms on the right hand side of Eq. (19) and the second and higher order contributions can be ignored. Using Eq. (18), we obtain

$$|j_i\rangle = \frac{1}{\sqrt{2}} \frac{1 + d}{1 + d} \frac{1}{\sqrt{2}} \frac{1}{\sqrt{2}} |j_i\rangle; \quad (20)$$

$$|j_i\rangle = \frac{1}{\sqrt{2}} \frac{1 - d}{1 + d} \frac{1}{\sqrt{2}} \frac{1}{\sqrt{2}} |j_i\rangle;$$

where

$$d = \frac{2 (f_q - 1/2) E_J}{\hbar L_j \sin[q_-]} |j_i\rangle$$

$$= \frac{2 (f_q - 1/2) E_J}{R R} \frac{L(q_+; q_-) L(q_+; q_-) \sin[q_-] d_{q+} d_{q-}}{(f_q) = 2} \quad (21)$$

and $L(q_+; q_-) = \hbar q_+; q_- |j_i\rangle$. Equation (20) clearly shows that the ground and the first excited states can be expressed as superposition of $|j_i\rangle$ and $|j_i\rangle$ even when the external ux deviates slightly from the degenerate point $f_q = 1/2$.

Therefore, we can simplify the qubit Hamiltonian H_q^0 as

$$H_q^0 = \sigma_z (f_q) \sigma_x \quad (22)$$

where σ_z and σ_x are the spin operators with the basis $|j_i\rangle, |j_i\rangle$. Although the above relations, Eqs. (21) and (22), were obtained perturbatively, their validity is confirmed by numerical calculations when f is comparable to f_q .

B. Effect of decoherence

Since we calculate the time evolution of the density operator of the qubit-SQUID coupled system, the effect of some types of decoherence can be easily taken into account. Here, we use a simple model of the decoherence, so called, the system-Boson model^{12,13}. The Hamiltonian for the system and the Boson environment is given by

$$H_{\text{tot}} = H + H_B + g A_S \sum_k (b_k^\dagger + b_k) + \sum_k \epsilon_k b_k^\dagger b_k; \quad (31)$$

with the interaction Hamiltonian $H_{SB} = \sum_k \epsilon_k (b_k^\dagger + b_k)$, where H is the Hamiltonian of the qubit-SQUID composite system given in Eq. (24), b_k is the annihilation operator of the Boson for the mode k , and g is the coupling constant, and A_S is the operator of a physical observable in the qubit-SQUID coupled system, which interacts with the environment. The time evolution of the density operator expressed by the influence functional manner, and it can be calculated numerically by, for example, the program established by Makris's group¹⁶. However, when it is allowed to approximate the effect of the interaction with the environment as a Markovian process, a simpler calculation can be performed, with the Lindblad equation¹⁷. Although if the effect of the non-Markovian character of the system-environment interaction is important, the Lindblad calculation might not be very useful^{18,19}, however, it gives suggestive results, as shown later, when the details of the origins of the decoherence in the experiments are unknown, as in the present case.

The Lindblad equation is given by

$$\frac{d}{dt} \rho(t) = \frac{1}{i\hbar} [H; \rho(t)] + \frac{\gamma}{2} (2A_S \rho(t) A_S^\dagger - A_S^\dagger A_S \rho(t) - \rho(t) A_S^\dagger A_S); \quad (32)$$

where γ is the coupling strength which is proportional to the square of g .

When (i) A_S / \sum_k , the decoherence destroys the quantum superposition between the $|L\rangle$ and $|R\rangle$ qubit states. This situation corresponds to the decoherence caused by the fluctuation of the external magnetic flux $\phi_q = \phi_q(0)$. (ii) A_S / ϕ_{0+} corresponds to the influence of the bias current I_b , the dissipation at normal resistance outside the SQUID. Moreover, (iii) $A_S / \phi_{0+} = \phi(t)$ expresses the detection of the finite voltage that appears across the SQUID. We will show the influence of this decoherence on the qubit-SQUID coupled system and the resulting switching currents by numerical calculations.

V. RESULTS AND DISCUSSION

A. Time evolution of the qubit-SQUID composite system during the measurement

We carried out numerical calculations of the time evolution of the density operator given by Eq. (25) of the

qubit-SQUID coupled system during the measurement.

First, in Fig. 3 we show the time evolution without decoherence, in other words, the pure unitary evolution of the $\phi_0 - z$ composite system. Time t is normalized by the inverse of the Josephson energy E_{J0} . The parameters for the numerical calculations are as follows. The Josephson energy and the capacitance of a SQUID junction are $E_{J0} = 100 \text{ GHz}$, and $C_0 = 40 \text{ fF}$, respectively. This gives $E_C = E_{J0} / 0.01$. The inductance of the SQUID ring is $L = 10 \text{ pH}$. The magnetic flux piercing the SQUID ring is $\phi_{SQ} = f_{SQ} \phi_0$ with $f_{SQ} = 0.4$. For the qubit, values of $\epsilon = 0.0065 E_{J0}$, and $\epsilon = 0.01 E_{J0}$ are given. These are almost the same as the experimental parameters used in the experiment by an NTT group¹⁰. We employed the mutual inductance $M = 1.4 L$, which gives approximately ten times greater qubit-SQUID coupling than in actual experiments carried out with the geometry shown in Fig. 2. Such strong coupling is chosen in order to distinguish the effect of the qubit state on the SQUID switching current within the precision of our numerical calculations. This interaction is still weak and does not change the discussion described later.

This set of parameters corresponds to a situation where $|L\rangle$ and $|R\rangle$ are almost degenerate. ($\epsilon \neq 0$ because the qubit-SQUID coupling shifts the degeneracy point.) At $t = 0$, we set the SQUID bias current $I_b = 0$, and the $\phi_0 - z$ composite system is in its ground state, that is, the bonding state of $|L\rangle$ and $|R\rangle$. For $t > 0$, I_b is increased much more slowly than the time scale related to other relevant energies. Actually, in this and later examples, the bias current increases at approximately $400 \text{ nA} / (\text{sec})$. This corresponds to the bias current reaching the switching current from zero in a time of about 0.1 sec .

The thin solid curves in Fig. 3 show the Josephson potential for ϕ_0 at each time. The thick solid curves show $p_L(\phi_0)$, and the thick dashed curves show $p_R(\phi_0)$, which are defined in Eq. (29). The initial state has amplitudes comparable for both the solid and dashed curves. This means that the initial qubit state is a superposition of $|L\rangle$ and $|R\rangle$. At this time, since $p_L(\phi_0) / p_R(\phi_0)$ is approximately satisfied, the qubit and the SQUID are not entangled. This is always the case when $I_b = 0$ regardless of the values of the parameters chosen.

With increasing I_b , the difference between $|L\rangle$ and $|R\rangle$ affects the position of the potential minimum in the coordinate ϕ_0 . As shown in the figure, without decoherence the relation $p_L(\phi_0) / p_R(\phi_0)$ is still largely maintained. Figure 4 shows this fact quantitatively. The quantity

$$R[L; R] = \frac{R}{\frac{p_L(\phi_0)}{d\phi_0} \frac{p_R(\phi_0)}{d\phi_0}} \quad (33)$$

for a pure state measures the degree of entanglement between the qubit and the SQUID. $R[L; R] = 1$, and 0 indicate no entanglement (separable) and maximum entanglement, respectively.

We can see that the quantity remains almost unity as the SQUID bias current I_b increases. By using this

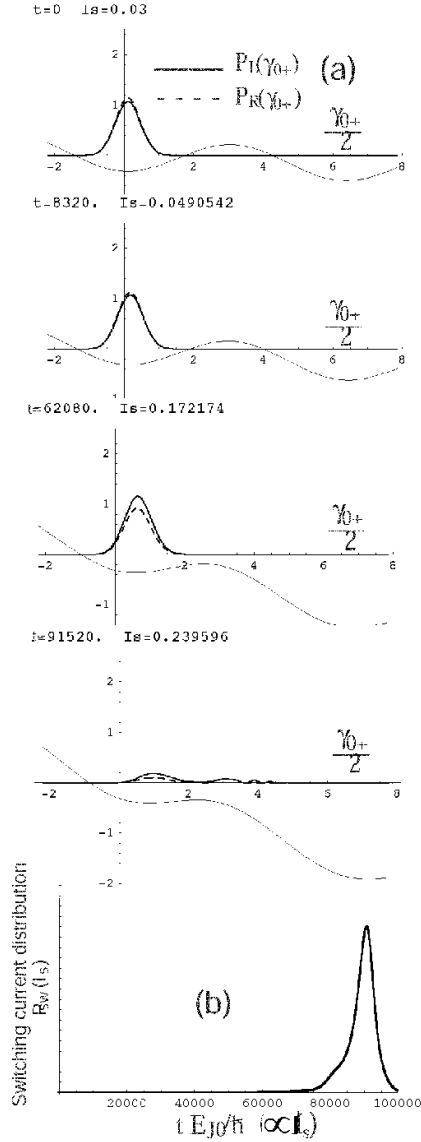


FIG. 3: Time evolution of the SQUID probability distribution without decoherence. $\gamma = 0.01 E_{J0}$. (a) Changes in the shape of the probability distribution. The solid curves show $p_L(\gamma_{0+})$ and the dashed ones show $p_R(\gamma_{0+})$ defined by Eq. (29). (b) Switching current distribution calculated by Eq. (30). The time t is proportional to the bias current $I_b(t)$, and normalized by the SQUID Josephson energy $h=E_{J0}$. $dI_b/dt = 400 \text{ nA}/(\text{sec})$.

quantity, the so called "entanglement of formation" is expressed as

$$E_{\text{formation}}^S(S_Q) = S(\rho_{\text{qubit}}) = -\frac{1}{2} \log_2 \left(\frac{1}{2} \left(1 + \sqrt{1 - 4R[L; R]} \right) \right); \quad (34)$$

where $S_Q = -\text{Tr}[\rho \log \rho]$ and $\rho_{\text{qubit}} = \text{Tr}_{\text{SQUID}}[\rho]$, and $S(\rho) = -\text{Tr}[\rho \log \rho]$ is the von Neuman entropy. Since

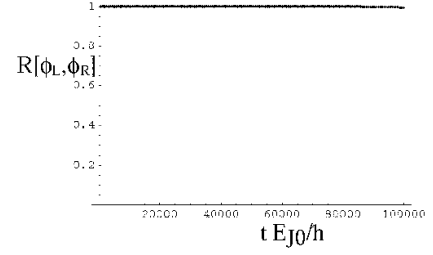


FIG. 4: Time evolution of the measure $R[L; R]$ of the entanglement between the qubit and the SQUID. $R = 1$ means no entanglement.

$2^{-R} d_{0+} j_L(\gamma_{0+})^2 d_{0+} j_R(\gamma_{0+})^2 < 1/2$ in Figs. 3, and 4, the entanglement of formation E is always kept below 0.1%.

The correlation between γ_z and γ_{0+} is formed by the interaction energy between the qubit and γ_{0+} . However, the entanglement makes it difficult to utilize the transfer energy between j_L and j_R of the qubit because the SQUID wavefunctions $\psi_L(\gamma_{0+})$ and $\psi_R(\gamma_{0+})$ are different when entangled, and the overlap between them becomes small. It is postulated that this fact suppresses the entanglement formation. In this situation the switching current may have an intermediate value between the values for j_L and j_R . The switching current distribution is shown in Fig. 3(b). It has only one significant peak.

B. What do we measure with a dc-SQUID?

In the vicinity of a half integer of f_q , the ground state $|g_i\rangle$ and the first excited state $|e_i\rangle$ of the qubit are

$$|g_i\rangle = a(f_q) |j_L\rangle + b(f_q) |j_R\rangle; \quad |e_i\rangle = b(f_q) |j_L\rangle - a(f_q) |j_R\rangle; \quad (35)$$

respectively. Here, we define

$$a(f_q) = \frac{q}{\sqrt{D}} \frac{1}{\sqrt{(f_q)^2 + \frac{1}{4} + (f_q)^2}}; \quad b(f_q) = \frac{1}{\sqrt{D}}; \quad D = \frac{1}{4} + (f_q)^2 + \frac{q^2}{(f_q)^2 + \frac{1}{4} + (f_q)^2}; \quad (36)$$

Since $(f_q) = 0$ at $f_q = 1/2$, $|g_i\rangle$ and $|e_i\rangle$ are superpositions of $|j_L\rangle$ and $|j_R\rangle$ at $f_q = 1/2$. Therefore, γ_z , which is proportional to the flux induced by the qubit circulating current, has large quantum fluctuations, and does not have a definite value. Then, what the dc-SQUID switching current I_{sw} measuring the induced flux corresponds to is ambiguous.

A simple explanation of the γ_z projection measurement is as follows. It requires not only classical correlation but also quantum entanglement between the SQUID and the qubit. When the interaction between the qubit and the SQUID produces entanglement between them, as given by Eq. (26), the wavefunctions $\psi_L(\gamma_{0+})$ and

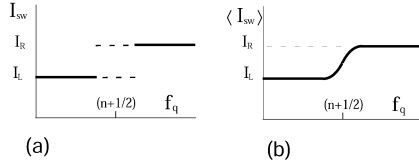


FIG. 5: Schematic of dc-SQUID switching current distribution according to a "projection" measurement of the qubit. (a) Before averaging. (b) Average value.

$|L\rangle$ and $|R\rangle$ have their peaks at different positions, f_{qL} and f_{qR} . As the SQUID bias current is increased, and when one of their wavefunctions reaches its switching point, it switches probabilistically. Therefore, if the two peaks are adequately separated in the coordinate f_q , we may find two peaks in the switching current distribution.

We denote the I_{sw} for $|L\rangle$ and $|R\rangle$ as I_L and I_R , respectively. According to a simple measurement formulation, the above is a f_q measurement. Then, if the simple formulation were correct, the measurement should give

I_L with the probability $p_L(f_q)$, I_R with the probability $p_R(f_q)$.

This is a probabilistic phenomenon, and therefore, the obtained values have a large distribution. These two peaks positioned at I_L and I_R appear in the plot of a huge number of obtained values. After averaging the values, the expectation value

$$\langle I_{sw} \rangle = \int I_{sw} p(f_q) df_q = p_L(f_q) I_L + p_R(f_q) I_R \quad (37)$$

would be obtained. This is shown schematically in Fig. 5.

If the measurement with the SQUID were a projection measurement of f_q as described above, the observed switching current would appear at a value corresponding to I_L or I_R , probabilistically. Therefore, if I_L were not proportional to I_R and $R[I_L; I_R] \neq 1$, the switching current would split into two values even for a one qubit state at absolute zero temperature, as sketched in Fig. 5(a).

In the experiment reported by the Delft group³, (perhaps for a reason that has nothing to do with qubit quantum fluctuations) the I_{sw} had a broad distribution, which prevents one even from distinguishing I_L and I_R on a single measurement basis. Therefore, they showed only the averaged values, which faithfully reproduced the curve shown in Fig. 5(b).

However, as described above, when we carried out numerical calculations on the time evolution of the density operator of the total system, we found that the total system wavefunction with low energies does not adopt an entangled state but remains almost separable, that is, $R[I_L; I_R] \approx 1$ ($I_L \approx I_R$). Only the position in the f_q coordinate of the wavepacket (f_q) depends on the qubit state. The obtained switching

current corresponds to that of $|f_q\rangle$, which is single-valued, unlike the entangled state mentioned above. In addition, the numerical calculation also showed that the switching current has a two-valued distribution in the presence of strong decoherence, which destroys the qubit superposition, as we will discuss in Figs. 7, and 11. Since the qubit circulating current I_{cir} is proportional to the z -component of the qubit spin, it should be written as $I_{cir} = I_{c0} \langle \sigma_z \rangle$, under the two-state approximation for the qubit. According to quantum mechanics, when the spin is in a superposition state $|\psi\rangle = a|L\rangle + b|R\rangle$, each f_q measurement provides the discrete result -1 or 1 probabilistically, and never provides an intermediate value. Although the quantum mechanically averaged value of the circulating current for the superposition state $|\psi\rangle = a|L\rangle + b|R\rangle$ is given by $\langle I_{cir} \rangle = I_{c0} 2ab$, this value is obtained after we measure I_{cir} for the state $|\psi\rangle$ many times and calculate its average value.

Very recently, the NTT group has succeeded in performing single-shot detection of the qubit flux by improving the switching current resolution in their SQUID¹⁰. The plots of the raw values of the switching currents clearly show the qubit state transition from the ground state to the first excited state accompanied by a change in the external magnetic field $f_q = f_{q0}$, without any averaging of the data¹⁰. One of the most interesting facts in their data is that the switching currents illustrate a curve that explicitly shows that the qubit is in a superposition of $|L\rangle$ and $|R\rangle$ in the vicinity of a degenerate point $f_q = 1.5$. In such a region, their switching currents appear at intermediate values between the switching currents for $|L\rangle$ and $|R\rangle$. A curve that is very similar to that in Fig. 5(b) appeared from the single shot data. The behavior of the switching current versus the external flux in Fig. 5(b) is very similar to that of the quantum mechanically averaged value of the qubit circulating current $\langle I_{cir} \rangle$ in Fig. 2(b). At first glance, this is very strange if we adopt the above simple formulation of the dc-SQUID measurement, which gives a two peak I_{sw} distribution for a superposed qubit state.

However, taking an experimentally realistic weak qubit-SQUID interaction into account in the Hamiltonian of the composite system, one finds that no entangled state between the qubit and the SQUID is formed. The time evolution keeps the composite system to be in a direct product state even in the presence of the interaction;

$$|\psi_{tot}\rangle = |\psi_{sq}\rangle |\psi_q\rangle \quad (38)$$

The qubit state affects the shape of the SQUID wavefunction;

$$|\psi_q\rangle = \sum c_n |n\rangle \quad (39)$$

The position of the peak of the wavefunction $|\psi_q\rangle$ varies with the qubit state although the wavefunction is a wavepacket with a finite width.

C. Variational analysis of the entanglement formation between the qubit and the SQUID

Entanglement formation in time is too complicated to examine analytically. Therefore, here, we consider the behavior of the entanglement in the ground state of the qubit-SQUID coupled system by using a variational calculation.

We adopt the trial wavefunction

$$\begin{aligned} \psi_{\text{trial}} = & \frac{2}{a} \int_{-a/2}^{a/2} dx \left[b_L e^{-\frac{(x-d_L)^2}{a}} \psi_{0+}(x) + b_R e^{-\frac{(x-d_R)^2}{a}} \psi_{0+}(x) \right] \quad (40) \end{aligned}$$

for the total system because the SQUID potential is nearly parabolic and the wavefunction in the potential should take the ground level. The width of the wave packet is a . We denote the difference between the peak positions of the L and R components as $d = (d_L - d_R)/2$, and midpoint between them by $(d_L + d_R)/2$. From the Hamiltonian (24), the expectation value $\langle H \rangle_{\text{trial}}$ of the energy for the trial wavefunction is given by

$$\begin{aligned} \langle H \rangle_{\text{trial}} = & \frac{E_C^0}{a} \int_{-a/2}^{a/2} dx \left[2e^{-a/8} E_{J0} \cos[f_{SQ} x] \cos[\phi_0] \cos d \right. \\ & \left. + e^{-a/8} E_{J0} k f \sin[\phi_0] \sin d \right] \cos[\phi_0] \cos d \\ & + e^{-2d^2/a} (b_L b_R + b_R b_L) \\ & + \frac{\hbar}{2e} \int_{-a/2}^{a/2} dx \left[\frac{1}{a} \left(\frac{d_L}{2} \right)^2 + \frac{1}{a} \left(\frac{d_R}{2} \right)^2 \right] \quad (41) \end{aligned}$$

where

$$k = \frac{M}{2} \frac{2e}{\hbar} E_{Jb} \sin[f_{SQ}]; \quad (42)$$

is the dimensionless qubit-SQUID coupling constant, and

$$E_C^0 = \frac{(2e)^2}{2C_0}; \quad (43)$$

Here k is of the order of 10^{-3} when we use the parameters in experiments^{3,10}. Therefore, we disregard the higher powers of k in the calculations below. Here, we ignored the self-energies for the qubit and the SQUID induced by the interaction, to simplify the discussion of the entanglement formation.

We minimize Eq. (41) with respect to the peak positions d_L and d_R , and the width of the wavefunction a , using an approximation that disregards k^2 , d^3 , a^3 and higher powers. Then, we obtain the minimum

$$\begin{aligned} \text{Min}_{d_L, d_R, a} \langle H \rangle_{\text{trial}} = & \frac{E_C^0}{a_0} + \frac{1}{a_0} \int_{-a_0/2}^{a_0/2} dx \left[\frac{1}{1+x^2} \right. \\ & \left. + \frac{2e}{\hbar} (1+xk^0) \int_{-a_0/2}^{a_0/2} dx \left[\frac{1}{I_0^2} + \frac{1}{I_b(t)^2} + \frac{1}{I_b(t)} \arcsin \left[\frac{I_b(t)}{I_0} \right] \right] \right] \quad (44) \end{aligned}$$

where

$$I_0 = \frac{2e}{\hbar} e^{-a_0/8} E_{J0} 2 \cos[f_{SQ}]; \quad (45)$$

$$x = \frac{d_L - d_R}{a}; \quad \frac{1}{1+x^2} = b_L b_R + b_R b_L; \quad (46)$$

$$k^0 = \frac{k}{2 \cos[f_{SQ}]}; \quad (47)$$

This minimum is realized when the peaks are positioned at

$$\frac{0+}{2} = d_L = d_0 + d_0; \quad \frac{0+}{2} = d_R = d_0 - d_0; \quad (48)$$

where

$$d_0 = \arcsin \left[\frac{I_b(t)}{I_0} \right] \frac{1}{\sqrt{1 - \frac{I_b(t)^2}{I_0^2}}} \frac{k^0 x \frac{4}{a_0} \frac{2e}{\hbar}}{\sqrt{1 - \frac{I_b(t)^2}{I_0^2}} + \frac{4}{a_0} \frac{2e}{\hbar}}; \quad (49)$$

$$d_0 = \frac{1}{\sqrt{1 - \frac{I_b(t)^2}{I_0^2}}} \frac{1}{\sqrt{1 - \frac{I_b(t)^2}{I_0^2}} + \frac{4}{a_0} \frac{2e}{\hbar}}; \quad (50)$$

and

$$a_0 = \frac{E_C^0}{(2E_{J0} \cos[f_{SQ}])^2 + \frac{1}{I_b(t)^2} + \frac{4}{a_0} \frac{2e}{\hbar}}; \quad (51)$$

This split between peaks $d_0 (\neq 0)$ is much smaller than the difference between the peak positions $d_0 (= 0)$ for the simple (not superposed) ψ_L and ψ_R . In fact, the ratio is given by

$$\frac{d_0}{d_0 (= 0)} = \frac{\frac{1}{\sqrt{1 - \frac{I_b(t)^2}{I_0^2}}} \frac{1}{\sqrt{1 - \frac{I_b(t)^2}{I_0^2}} + \frac{4}{a_0} \frac{2e}{\hbar}}}{\frac{1}{\sqrt{1 - \frac{I_b(t)^2}{I_0^2}}} \frac{1}{\sqrt{1 - \frac{I_b(t)^2}{I_0^2}} + \frac{4}{a_0} \frac{2e}{\hbar}}}; \quad (52)$$

This ratio becomes vanishingly small as the bias current approaching the switching current, that is, $I_b \rightarrow I_0$. Therefore, when the qubit superposition exists, the entanglement between the qubit and the SQUID is negligible, at least just before the switching. At that time, Eq. (49) gives the position of the SQUID wavefunction peak at

$$x = \arcsin \left[\frac{I_b}{I_0} \right] \frac{1}{\sqrt{1 - \frac{I_b^2}{I_0^2}}}; \quad (53)$$

This coincides with the peak position when the qubit has a classically definite spin $\sigma_z = x$.

Finally, we can estimate by an approximate variational calculation that the peak of the SQUID wavefunction is positioned at

$$\sigma_z \neq x = \frac{d_L - d_R}{a} = \frac{2d_0}{a} \approx \frac{2}{a} \arcsin \left[\frac{I_b}{I_0} \right] \frac{1}{\sqrt{1 - \frac{I_b^2}{I_0^2}}}; \quad (54)$$

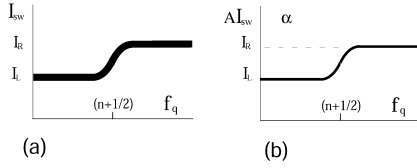


FIG. 6: Schematic dc-SQUID switching current distribution according to a "weak" measurement of the qubit. (a) Before averaging. (b) Average value.

when the qubit is in a superposed state $|j_q\rangle = a|j_L\rangle + b|j_R\rangle$ unless the state of the qubit undergoes a rapid change. This coincides with the quantum mechanical average $\langle j_q \rangle$ of $|j_q\rangle$. Therefore, in the absence of decoherence, we can interpret this to mean that the resulting switching current value, at which the $|j_q\rangle$ escapes from the Josephson potential, coincides with the quantum-mechanical average $\langle I_{sw} \rangle$ before any averaging operation.

D. Effect of decoherence

The discussion in Sec. V B becomes more convincing when we compare the time evolution in Fig. 7 with decoherence.

When we use unrealistically strong coupling between the qubit and the SQUID, there is a significant entanglement. However, this still gives only one peak in the switching current distribution in our calculation. This shows that entanglement by itself does not cause a two-value measurement, in other words, a z projection measurement. Nevertheless, such strongly entangled states are not robust against a weak decoherence, which destroys the qubit superposition and realistic switching current distribution for a strong interaction as discussed in this section.

Assuming a Markovian process, we performed the calculation using the Lindblad equation (32) with $A_S = z$ and $\gamma = 3 \times 10^{-4} E_{J0} / \hbar$. The decoherence makes the composite system a mixed state, and the states $|j_L\rangle$ and $|j_R\rangle$ become incoherent to each other. Therefore, the transfer energy between $|j_L\rangle$ and $|j_R\rangle$ through ϕ does not matter any longer, and the interaction between the qubit and the SQUID determines the state of the system resulting in the qubit state dependence of the SQUID wavefunction shape. In this situation, however, the qubit-SQUID correlation is not an entanglement but a classical correlation because the states with different qubit states are already incoherent to each other. In terms of Eqs. (27)–(29) of the density operator, the L component ρ_{LL} and the R component ρ_{RR} belong to different $|j_L\rangle, |j_R\rangle$ ($i \neq j$). The switching current value becomes one for $|j_L\rangle$ or for $|j_R\rangle$ in a probabilistic manner. This appears in the switching current distribution in Fig. 7(b). The peak is split into two, corresponding to $|j_L\rangle$ and $|j_R\rangle$, respectively.

This type of peak splitting in the switching current

distribution caused by the decoherence occurs when the qubit superposition is weak (γ is small), or/and when the qubit-SQUID interaction energy is so large that a strong qubit-SQUID entanglement is formed before the decoherence makes the system a mixed state.

Our formulation can readily be used to investigate another type of decoherence. Although we do not show the results of our numerical calculations here, we briefly comment on some of them. When the quantity of the system that couples with the environment is the SQUID ϕ_0 or $\phi_0/2$, the interaction between the system and the environment does not directly deteriorate the qubit superposition between $|j_L\rangle$ and $|j_R\rangle$. Since the qubit-SQUID coupling through the mutual inductance is weak in the above calculations (and experiments), the environment deforms only the shapes of the SQUID wavefunction. This makes the qubit-SQUID system a mixed state. However, each eigenstate of the mixed-state density operator of the $|j_L\rangle, |j_R\rangle$ superposed qubit is largely maintained even if the coupling to the bath is strong. Although the switching current distribution of the mixed-state density operator may sometimes have several peaks, the splitting of the peak does not correspond to the splitting of the qubit into $|j_L\rangle$ and $|j_R\rangle$. The peaks instead correspond to different SQUID states, for example, the ground and first excited states of the Josephson plasma oscillation.

E. Switching current behavior with a change in the external magnetic flux ϕ_q

If the above discussion of what is indicated about the qubit by the switching current is correct, our theory must reproduce the switching current behavior observed in experiments with the change of the external magnetic flux ϕ_q ($/ f_q$) shown in Fig. 6. We carried out a time-evolution calculation at various f_q values and present the results in Figs. 8, 9, and 10.

Figures 8 and 9 show the switching current behavior with the energy splitting ϵ between $|j_L\rangle$ and $|j_R\rangle$ when there is no decoherence. Since ϵ is proportional to the deviation of the external magnetic flux from the degenerate point $f_q = (n + 1/2)$, as shown in Eq. (21), the horizontal axis also corresponds to the change in f_q . The peak position of the switching current distribution gradually shifts from I_L to I_R , and there is no discontinuous transfer. This suggests that the switching current traces a continuous curve as shown by the schematic illustration in Fig. 6.

Figure 11, where the peak positions of the switching current distributions for various external fluxes are plotted, shows clearly that the ϵ dependence of I_{sw} obeys such a law. Without decoherence I_{sw} gradually transfers from the switching current for $|j_L\rangle$ to $|j_R\rangle$ across the degenerate point ($\epsilon = 0$). By contrast, I_{sw} suddenly jumps from one for $|j_L\rangle$ to $|j_R\rangle$ at the degenerate point and two peaks appear at certain flux values. The circles indicated by arrows are the I_{sw} values of the same parameter sys-

tem for various decoherence strengths. This provides evidence that a measurement giving a single intermediate I_{sw} is changed into a two-value measurement by strong decoherence.

F. Comment on the precision of a single measurement

The problem analyzed here is invoked by our experiment where each single switching current measurement has sufficient resolution to distinguish whether the qubit is in $|L\rangle$ or $|R\rangle$. If we could not obtain the switching current behavior depending on the external flux, it would not make us aware of the importance of understanding the switching currents that appear in the intermediate region between I_L (for $|L\rangle$) and I_R (for $|R\rangle$) because the averaged value of the projection measurement results always gives the intermediate value when the qubit is in a superposition state. Therefore, here, we briefly consider the factors that determine the resolution of the switching currents.

As we have discussed in this paper, the quantum fluctuations in the qubit-induced flux ϕ_q , in other words, the quantum fluctuations of ϕ_z , are not directly related to the SQUID resolution. Within the precision of our numerical calculation, there is no significant difference between the half width of the switching current distribution for a ϕ_z definite state and a superposition state. In our numerical calculation, we found that the distribution width increased when we used a larger SQUID junction capacitance. When the capacitance is large, the level splitting of the SQUID plasma oscillation of ϕ_+ is narrow, so the increase in the SQUID bias current excites the plasma oscillations. As the result, the state of ϕ_+ is distributed over many levels that have slightly different switching currents. Therefore, the distribution becomes broader resulting in a poorer resolution. This fact does not identify the origin of the high resolution of our measurement because there are many other factors that cause those changes in the distribution width, including the speed of the increase in the bias current, and the strength of decoherence. The resolution problem is still an open question.

VI. CONCLUSION

We discussed the superconducting flux-qubit measurement with a dc-SQUID from the viewpoint of the dynamics of a composite system consisting of a qubit and a SQUID. Since both the qubit and SQUID are quantum systems the relation between the measured object (qubit state) and the outcome (switching current) of the measurement apparatus is not trivial.

We calculated the time evolution of the density operator of a qubit-SQUID coupled system from the onset of

an increase in the bias current to the switching event, and examined the behavior of the switching current distribution.

Of particular interest is the fact that when the ground state of the composite system is a qubit superposition state, the measurement designed to distinguish in which state the qubit is does not always work as designed, and there is a possibility that the switching current will have an intermediate value between the two states. Nevertheless, even in such a situation, when there is decoherence (reduction in the off-diagonal elements of the density operator) which destroys the qubit superposition of $|L\rangle$ and $|R\rangle$, the switching current then gives us information about $|L\rangle$ or $|R\rangle$ in a probabilistic manner.

When the external field ϕ_q is far from the degenerate point ($\phi_q = (n + 1/2)\phi_0$), since there is no quantum transfer between the two states of the qubit, the qubit should be in the lower energy state, and the switching current of the SQUID shows a value corresponding to that state. The switching current I_{sw} is different for $\phi_q < (n + 1/2)\phi_0$ and $\phi_q > (n + 1/2)\phi_0$ because the energies of the two states cross at the degenerate point.

We find by variational calculation that the peak position of the wavepacket (ϕ_+) is approximately the bottom of the SQUID Josephson potential $V_{SQ}(\phi_+; \phi_z = 2\pi\hbar^2/2e\Phi_0)$. The resulting switching current becomes that for a usual magnetic field measurement with SQUID of this potential. This value coincides with the quantum-mechanical average $\hbar I_{sw}$ of the switching current for the qubit $j_q = a|L\rangle + b|R\rangle$. The fact that the switching current behaves as the average value, which may at first seem strange, is explained as described above. Moreover, this indicates a very important fact about the dc-SQUID measurement of flux-qubit states. The measurement is not a projection measurement that determines whether the qubit is $|L\rangle$ or $|R\rangle$. It is a simple measurement of the weight $|a|^2 (= 1 - |b|^2)$ of the qubit.

The flux ϕ_q induced by the qubit ring current has a large quantum fluctuation when the qubit is in a superposition state. The fluctuation of the measured switching current, however, has almost nothing to do with the fluctuation of ϕ_q . The switching current fluctuation is caused mainly by fluctuations of the SQUID itself.

Our theoretical results in the present work clearly explain the switching current behavior revealed by our experimental results. This may provide us with important clues to improve the measurement scheme for quantum computations.

Acknowledgments

We thank S. Ishihara for his encouragement throughout this work. We also thank A. Shnirman and C. J. P. Harmans, and D. Esteve, for their helpful comments. We also acknowledge J. E. Mooij, C. van der Wal, Y. Nakamura, and M. Devoret for useful discussions.

- ¹ M. A. Nielsen and I. L. Chuang, 'Quantum Computation and Quantum Information', (Cambridge Univ. Press, 2000).
- ² J. R. Friedman, V. Patel, W. Chen, S. K. Tolpygo, and J. E. Lukens, Nature 406, 43 (2000).
- ³ C. van der Wal et al., Science 290, 773 (2000).
- ⁴ J. M. Martinis, S. Nam, J. Aumentado, and C. Urbina, Phys. Rev. Lett. 89, 117901 (2002).
- ⁵ C. van der Wal, 'Quantum superpositions of persistent Josephson currents,' Ph.D. thesis, Delft Univ. Press (2001).
- ⁶ I. Chiorescu, Y. Nakamura, C. J. P. M. Hamers, J. E. Mooij, Science 299, 1869 (2003).
- ⁷ Y. Nakamura, Yu. A. Pashkin, and J. S. Tsai, Nature 398, 786 (1999).
- ⁸ Y. Yu, S. Han, X. Chu, S. Chu, and Z. Wang, Science 296, 889 (2002).
- ⁹ D. Vion, et al., Science 296, 886 (2002).
- ¹⁰ H. Tanaka, Y. Sekine, S. Saito, H. Takayanagi, Physica C 368, 300 (2002); H. Takayanagi, H. Tanaka, S. Saito, and H. Nakano, Physica Scripta T 102, 95-102 (2002); H. Tanaka, S. Saito and H. Takayanagi, p. 366 in 'Toward the Controllable Quantum States', edited by H. Takayanagi and J. Nitta (World Scientific Pub., Singapore, 2003).
- ¹¹ J. E. Mooij, et al., Science 285, 1036 (1999).
- ¹² U. Weiss, 'Quantum Dissipative Systems' 2nd edition, (World Scientific pub., Singapore, 1999).
- ¹³ A. J. Leggett, Prog. Theor. Phys. Suppl. 69, 80 (1980); A. O. Caldeira and A. J. Leggett, Phys. Rev. Lett. 46, 211 (1981); A. O. Caldeira and A. J. Leggett, Ann. Phys. 149, 374 (1983).
- ¹⁴ H. Nakano and H. Takayanagi, J. of Phys. Soc. Jpn, Suppl. A 1 (2003); H. Nakano and H. Takayanagi, p. 359 in 'Toward the Controllable Quantum States', edited by H. Takayanagi and J. Nitta (World Scientific Pub., Singapore, 2003).
- ¹⁵ R. P. Feynman and F. L. Vernon, Annals of Phys. 24, 118 (1963).
- ¹⁶ N. M. Akri, J. Math. Phys. 36, 2430 (1995).
- ¹⁷ G. Lindblad, Commun. Math. Phys. 48, 119 (1976).
- ¹⁸ Lin Tian, S. Llyd and T. P. Orlando, Phys. Rev. B 65, 144516 (2002).
- ¹⁹ C. H. van der Wal, F. K. Wilhelm, C. J. P. M. Hamers, J. E. Mooij, Eur. Phys. J. B 31, 111 (2003).

APPENDIX A: ELIMINATION OF VARIABLES, ϕ_0 AND q_3

Here, we briefly explain how we eliminate invisible variables, ϕ_0 and q_3 .

Picking up terms including ϕ_0 or ϕ_0 from the Hamiltonian Eq. (5), we obtain

$$H(\phi_0) = \frac{1}{2} m \dot{x}^2 + \frac{1}{2} m \phi_0^2 x^2 + x F(t) - 2E_{J0} \cos[\phi_0 + 2] \sin[f_{SQ}]; \quad (A1)$$

where

$$m = \frac{C_0}{2} + \frac{h}{2e} \dot{x}^2; \quad (A2)$$

$$x = \phi_0 + 2 f_{SQ}; \quad (A3)$$

$$S = \frac{2L_q}{C_0 (L_q L + M^2)} \frac{2e}{h} \frac{2E_{J0}}{C_0} \cos[\phi_0 + 2] \cos[f_{SQ}]; \quad (A4)$$

$$F(t) = \frac{h}{2e} \frac{M}{L_q L + M^2} \dot{q}(t) + E_{J0} \cos[\phi_0 + 2] \sin[f_{SQ}]; \quad (A5)$$

$$q = q_1 + q_3 + 2 f_q; \quad (A6)$$

Here, we neglected x^3 and higher powers such as $\cos[x]!$ because x is strongly constricted in the parabolic potential.

Then, the Feynman-Vernon influence functional expressing the effect of ϕ_0 on the motion of $F(t)$ is given by^{12,15}

$$F_{FV} = \exp[-F_{FV}]; \quad (A7)$$

where

$$F_{FV} = \frac{1}{h} \int_0^t dt_1 \int_0^{t_1} dt_2 [F(t_1) - F^0(t_1)] [L(t_1 - t_2) F(t_2) - L(t_1 - t_2) F^0(t_2)]; \quad (A8)$$

$$L(t) = \frac{1}{2m \phi_0} \coth \frac{h \phi_0}{2} \cos[\phi_0 t] \sin[\phi_0 t]; \quad (A9)$$

Carrying out the t_2 integration in Eq. (A8) by parts, two times,

$$\begin{aligned} & \int_0^{t_1} dt_2 [L(t_1 - t_2) F(t_2) - L(t_1 - t_2) F^0(t_2)] \\ &= \frac{1}{2m \phi_0^2} [i(F(t_1) + F^0(t_1)) \cos \phi_0 t_1 (F(0) + F^0(0)) \\ & \quad + \coth \frac{h \phi_0}{2} \sin \phi_0 t_1 (F(0) - F^0(0)) \\ & \quad + \frac{1}{2m \phi_0^3} \sin \phi_0 t_1 (F(0) + F^0(0)) + \coth \frac{h \phi_0}{2} \end{aligned}$$

$$\cos \phi_0 t_1 (F(0) - F^0(0)) - F(t_1) - F^0(t_1)]$$

$$\frac{1}{\phi_0^2} \int_0^{t_1} L(t_1 - t_2) F(t_2) dt_2 - \int_0^{t_1} L(t_1 - t_2) F^0(t_2) dt_2; \quad (A10)$$

is given. Here, $F(t)$ indicates the quantity on the forward line and $F^0(t)$ that on the backward one. ~~A'~~

and A' mean the first and the second time derivatives of the quantity A , respectively. Since $F(t) = \frac{\hbar^2}{2e} \frac{M}{L_q L} \frac{1}{M^2} \varphi(t) = \frac{E_{J0}}{2} \sin[\varphi_0 + 2] \sin[f_{SQ}]_{\varphi_0}$, and both $\varphi(t)$ and φ_0 are of the order of $\frac{E_J E_C}{\hbar}$ at most, the terms from the second line of Eq. (A10) are smaller by the factor $\frac{E_J E_C}{\hbar} = (\hbar \Gamma_0) \frac{2e}{\hbar} \frac{1}{L E_{J0}}$ than those in the first line. This factor is no larger than 10^{-1} in experiments^{3,5,10}, therefore, we only take the terms in the first line in Eq. (A10).

Now we obtain

$$F_V = \frac{1}{2\hbar m \Gamma_0^2} \int_0^Z dt_1 [F(t_1) - F^0(t_1)] \\ i(F(t_1) + F^0(t_1)) \cos \Gamma_0 t_1 (F(0) + F^0(0)) \\ + \coth \frac{\hbar \Gamma_0}{2} \sin \Gamma_0 t_1 (F(0) - F^0(0)) : \quad (A11)$$

Highly oscillatory terms such as, $\sin \Gamma_0 t_1$, $\cos \Gamma_0 t_1$ are suppressed by the integration over t_1 . This enables us to neglect these terms.

Finally, we obtain the influence functional

$$F_{FV} = \exp \frac{i}{2\hbar m \Gamma_0^2} \int_0^Z dt_1 [F(t_1) - F^0(t_1)] [F(t_1) + F^0(t_1)] \\ = \exp \frac{i}{2\hbar m \Gamma_0^2} \int_0^Z dt_1 [F(t_1)^2 - F^0(t_1)^2] \\ = \exp \frac{i}{2\hbar m \Gamma_0^2} \int_0^Z F(t_1)^2 dt_1 \\ \exp \frac{i}{2\hbar m \Gamma_0^2} \int_0^Z F^0(t_1)^2 dt_1 : \quad (A12)$$

This influence functional is local in time and $F(t_1)$ and $F^0(t_1)$ are separated so that the effect of Γ_0 gives a unitary evolution which is expressed by the Hamiltonian

$$H = \frac{1}{2m \Gamma_0^2} F(t)^2 \\ = \frac{L_q L}{2L_q} \frac{M^2}{h} \frac{2e}{h} \frac{\hbar^2}{2e} \frac{M}{L_q L} \frac{1}{M^2} \varphi(t) + E_{J0} \cos[\varphi_0 + 2] \sin[f_{SQ}] \\ \quad (A13)$$

Very similarly, the elimination of φ_3 is carried out as follows. The Hamiltonian concerning φ_3 is

$$H(\varphi_3) = \frac{1}{2} m_Y \dot{Y}^2 + \frac{1}{2} m_Y \Gamma_1^2 Y^2 + F_Y(t) Y \\ \frac{L_q L}{2L_q} \frac{M^2}{h} \frac{2e}{h} E_{J0}^2 \cos^2[\varphi_0 + 2] \sin^2[f_{SQ}] \\ E_J \cos[\varphi_0 + 2] \varphi_3 + \frac{M}{L_q} E_{J0} \cos[\varphi_0 + 2] \sin[f_{SQ}]$$

$$+ \frac{1}{2} E_J \sin[\varphi_0 + 2] \varphi_3 + \frac{1}{2L_q} \frac{\hbar^2}{2e} (\varphi_0 + 2) \varphi_3^2; \quad (A14)$$

where

$$m_Y = C_q \frac{\hbar^2}{2e}; \quad (A15)$$

$$Y = \varphi_3; \quad (A16)$$

$$m_Y \Gamma_1^2 = E_J \sin[\varphi_0 + 2] \varphi_3 + \frac{1}{L_q} \frac{\hbar^2}{2e}; \quad (A17)$$

$$F_Y(t) = (\varphi_0 + 2) \varphi_3 + E_J \cos[\varphi_0 + 2] \varphi_3 + \frac{\hbar^2}{2e} \frac{1}{L_q} \\ \frac{M}{L_q} E_{J0} \cos[\varphi_0 + 2] \sin[f_{SQ}] + E_J \sin[\varphi_0 + 2] \varphi_3; \quad (A18)$$

Here, we neglected $(\varphi_3 + \varphi_0 + 2) \varphi_3^3$ and higher powers because they are strongly constricted in the parabolic potential. The influence functional expressing the effect of φ_3 on φ_0 and φ_0 is given from this description. Moreover, the terms that are non-local in time are negligible for the same reason as that for Γ_0 . Finally, we obtain the simplified Hamiltonian Eq. (12) where φ_3 and Γ_0 have been eliminated.

APPENDIX B: DISCRETE VARIABLE REPRESENTATION OF φ_0

Since the variable φ_0 is a continuous one, it is not directly suitable for numerical calculations. Therefore, we discretized them as follows.

The domain of φ_0 is restricted within $(a; b)$, where $a = 0.7$; $b = 2.5$. This domain is wide enough to express the SQUID wavefunction. We prepare orthonormal basis f_{j_n} ig, which satisfies $\langle \varphi_0 | f_{j_n} \rangle = \exp[i k_n (\varphi_0 - a)]$, where $k_n = 2\pi n / (b - a)$, $n = 0; 1; 2; \dots; N$. They are Fourier series and φ_0 eigenstates. From this set of f_{j_n} ig, we make φ_0 eigenstates

$$| \varphi_0 + j_m \rangle = \frac{1}{\sqrt{N}} \sum_{n=0}^{N-1} | j_m + n \rangle; \quad (m = 0; 1; 2; \dots; N); \quad (B1)$$

where

$$| j_m \rangle = \sum_n a_{m,n} | j_n \rangle; \quad \sum_n | a_{m,n} |^2 = 1; \quad (B2)$$

We use this basis f_{j_m} ig for the discrete variable representation of φ_0 and the wavefunction of the SQUID is expressed as the linear combination of $| j_m \rangle$. Using this

basis with finite N corresponds to the abandonment of the states of higher momentum energies in the SQUID. Therefore, we can calculate low energy states precisely

with small numbers of elements of the basis compared with other bases, such as $0+$ eigenstates placed with the same interval over $(a;b)$.

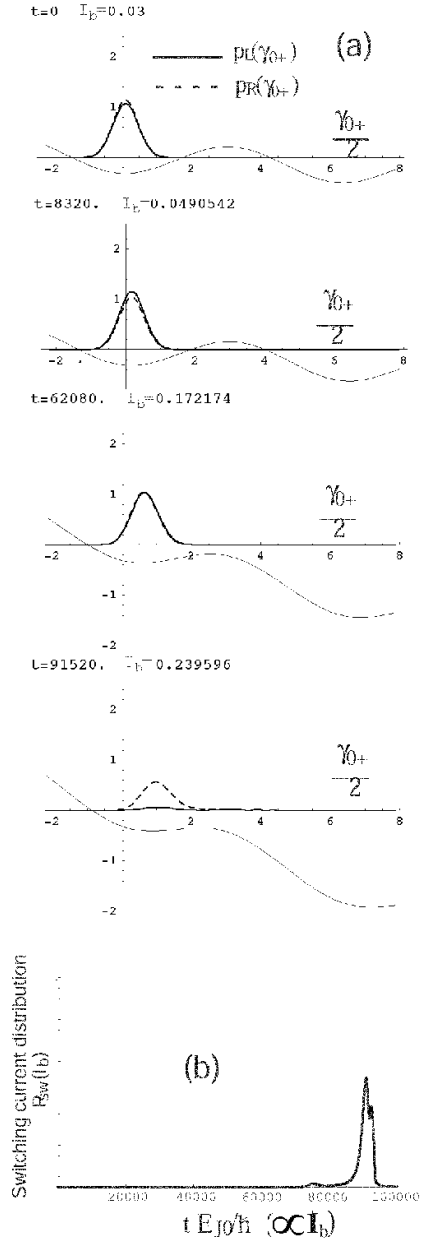


FIG. 7: Time evolution of the SQUID probability distribution with decoherence proportional to γ with $\gamma = 3.6 \cdot 10^{-4} E_{J0}/\hbar$, $\gamma = 0.001 E_{J0}/\hbar$. (a) Changes in the shape of probability distribution. The solid curves show $p_L(\gamma_{0+})$ and the dashed ones show $p_R(\gamma_{0+})$ defined by Eq. (29). (b) Switching current distribution calculated using Eq. (30). The time t is proportional to the bias current I_b , and is normalized by the SQUID Josephson energy $\hbar E_{J0}$. $dI_b/dt = 400$ nA/(sec).

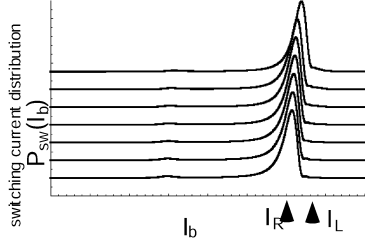


FIG. 8: Calculated dc-SQUID switching current distribution in the qubit measurement. ($\alpha = 0.01E_{J0}$) Each curve corresponds to the distribution for an energy difference Δ between J_L and J_R . The curves are vertically shifted for clarity. From top to bottom, $\Delta E_{J0} = 0.025; 0.015; 0.010; 0.0065; 0.0046; 0.002; + 0.005$.

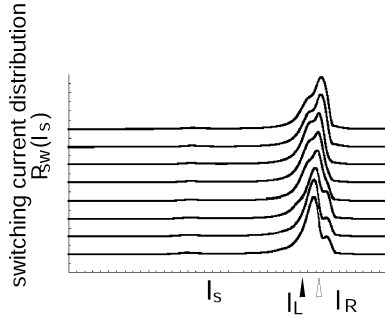


FIG. 9: Calculated dc-SQUID switching current distribution in the qubit measurement. ($\alpha = 0.01E_{J0}$) Each curve corresponds to the distribution for an energy difference Δ between J_L and J_R . The curves are vertically shifted for clarity. From top to bottom, $\Delta E_{J0} = 0.027; 0.025; 0.015; 0.010; 0.0065; 0.004; 0.002; + 0.005; + 0.007$.

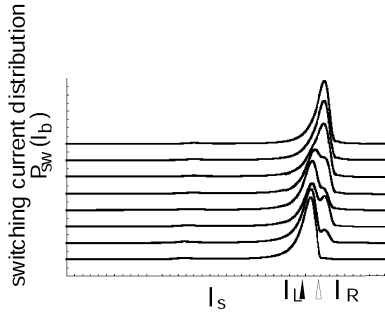


FIG. 10: Calculated dc-SQUID switching current distribution in the qubit measurement. ($\alpha = 0.001E_{J0}$) Each curve corresponds to the distribution for an energy difference Δ between J_L and J_R . The curves are vertically shifted for clarity. From top to bottom, $\Delta E_{J0} = 0.015; 0.010; 0.0065; 0.004; 0.002; 0.000; + 0.002; + 0.005$.

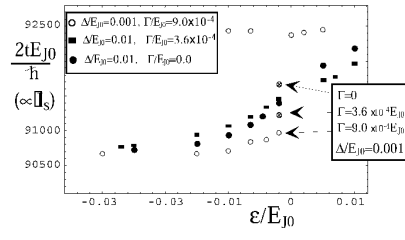


FIG .11: " dependence of the switching current peak position .